Open Access

Iraqi Journal of Industrial Research (IJOIR)

Journal homepage: http://ijoir.gov.iq

Comparative Assessment of Satellite and Field Surveying Data Accuracy for Construction Projects in Iraq

[1]Sahar S. Abdullah*, [1]Saad I. Hussein, [1]Wadah S. Mohiessen, [1]Ghada S. Kadhim, [2]Emad J. Mahdi

[1]Renewable Energy and Environment Research Center, Corporation of Research and Industrial Development, Iraq

[2]Ministry of Higher Education and Scientific Research, Scientific Research Commission, Iraq

Article information

Article history:
Received: November, 17, 2025
Accepted: January, 23, 2026
Available online: June, 14, 2026

Keywords:
Remote sensing,
Traditional land surveying,
Laser ranging,
GNSS measurements,
Statistical analysis

Corresponding Author:
Sahar S. Abdullah
saharsadoun9@gmail.com

DOI:
https://doi.org/10.53523/ijoirVol13I1ID625

Abstract

This study aims to evaluate whether freely available Sentinel-2 and Landsat-8 satellite imagery—when orthorectified using a local ground control point (GCP) network—can meet the positioning accuracy requirements of civil surveying for construction projects in Baghdad, Iraq, where economic sanctions and budgetary constraints preclude routine deployment of high-cost LiDAR systems. While satellite data offer broad coverage and low acquisition costs, their meter-scale geolocation errors often fall short of the centimeter-level precision required for legal boundary demarcation and structural design. To address this gap, we established a 25-point GCP network at the Corporation of Research and Industrial Development (CRID) site (59,600 m²) using TOPCON GR-5/GRS-1 GNSS and ES-105 total station, achieving a planimetric RMSE of 2.1 cm and vertical RMSE of 3.4 cm. These points were used to orthorectify Sentinel-2 and Landsat-8 imagery in ENVI 5.6 (FLAASH atmospheric correction, 2nd-order polynomial). Results show that GCP-constrained Sentinel-2 attained a horizontal RMSE of 6.8 m—an 85% improvement over raw data—while Landsat-8 stabilized at 12.4 m. Critically, this hybrid workflow reduced surveying costs by ~70% (from ~520 to 45 IQD/m²), without compromising boundary fidelity: the field-derived area (59,599.59 m²) matched official records (59,600 m²) within 0.4 m², whereas uncorrected satellite data overestimated the area by 499 m²,a discrepancy consistent with prior studies of urban cadastral applications. We conclude that while centimeter-grade field data remain essential for final design and legal documentation, GCP-enhanced Sentinel-2 offers a pragmatic, cost-efficient solution for preliminary planning, corridor mapping, and rapid cadastral updates in Iraqi urban settings.

1. Introduction

Geospatial data quality fundamentally governs civil engineering design reliability for urban infrastructure. In Iraq, economic sanctions preclude advanced LiDAR acquisition, necessitating evaluation of freely available Sentinel-2 (10m GSD) and Landsat-8 (30m GSD) against conventional field instruments [1]. Baghdad's 4.2% annual urban expansion [2] demands cost-effective solutions balancing accuracy, coverage, and affordability.

While literature confirms GNSS/Total Station centimeter-level superiority over satellite meter-scale precision [3], Iraq-specific cost-benefit analyses remain absent. This study addresses this gap through:

1) CRID site (59,600 m²) accuracy quantification
2) ENVI 5.6 orthorectification validation (25 GCPs)
3) Hybrid methodology demonstrating 70% cost reduction [4].

The quality of geographic data is essential for all Construction Projects, as it is a decisive factor in the design and planning of infrastructure projects such as roads, bridges, and drainage systems. With advances in technology, remote sensing has become a key approach for collecting spatial data by combining field measurements (total stations, laser distance meters, high-precision GNSS devices) with multispectral images from Sentinel and Landsat satellites, achieving wide spatial coverage while reducing field survey time and resource requirements. However, these technologies still face challenges related to data accuracy, acquisition cost, and coverage extent, which directly affect the quality of digital terrain models and the reliability of engineering designs. While field measurements can achieve centimeter-level accuracy, satellite data often exhibit errors ranging from several meters to tens of meters, especially in areas with complex terrain, dense vegetation, or persistent cloud cover. Traditional field surveying is also more expensive, labor-intensive, and time-consuming than satellite-based mapping, prompting the development of hybrid solutions that combine available field instruments with satellite data to achieve a better balance between accuracy, cost, and coverage [5-9].

Ground control points (GCPs) are widely used to improve the georeferencing of satellite data and link image coordinates to field observations. To obtain effective GCPs, measurements must be collected with high accuracy and distributed appropriately across the site. Construction Projects typically integrate various remote sensing sources, including satellite imagery (such as Landsat and Sentinel), aerial photography, drone surveys, LiDAR point clouds, and SAR data, to support terrain modeling and infrastructure planning [10, 11].

Geospatial data is fundamental to all surveying, civil engineering, and geodetic tasks, as the reliability of infrastructure designs—such as roads, bridges, and sewage networks—rests upon the integrity of spatial information. Remote sensing technologies have emerged as crucial sources, offering broad spatial coverage and timely updates through satellite imagery (e.g., Sentinel, Landsat) and airborne systems. However, these methods generally provide less accuracy than ground-based observations obtained using total stations or high-precision GNSS equipment.

To evaluate the practicality of such datasets, several quality metrics are considered: spatial accuracy (how correctly locations are represented), spectral resolution (capacity to distinguish land cover types), temporal resolution (frequency of image acquisition and monitoring), radiometric stability, and the precision of derived measurements such as elevation, distance, and volume. While LiDAR solutions enable highly detailed digital elevation models due to their superior spatial and vertical accuracy, high costs often limit their deployment. Conversely, freely available Sentinel-2 and Landsat-8 images offer more affordable and regularly updated coverage, though their positional accuracy is limited to several meters, sometimes falling short for demanding engineering purposes.

As a result, the field is moving toward hybrid strategies that combine remote sensing data with accurate ground-based measurements to optimize accuracy, costs, and spatial reach [12-18].

Collectively, these studies affirm that field instruments remain essential for legal boundary definition, while GCP-corrected Sentinel-2 offers a pragmatic alternative for planning. Yet, to date, no published work has benchmarked Sentinel-2 or Landsat-8 against a high-precision GCP network in an Iraqi urban context—nor quantified unit-cost savings relative to full-field surveying. This gap is critical, as Okolie & Smit (2022) and Zhang et al. (2019) both stress the need for *context-specific validation* before scaling satellite-based methods in infrastructure projects [18],

This study directly addresses that void: it presents the first Iraqi field validation of *independently processed* Sentinel-2 and Landsat-8 imagery—*not fused or AI-enhanced*—against a 25-point GCP network, with explicit cost–accuracy trade-offs for construction project workflows.

1.1. Previous Studies

Extensive research in geospatial and remote sensing demonstrates that data quality strongly influences surveying and engineering applications. Numerous studies highlight that integrating high-resolution laser scanning or LiDAR with GIS and GNSS/total station data enhances the fidelity of 3D city models, digital elevation models, and topographical maps, resulting in more dependable outcomes for urban planning and asset management [19-22].

Recent research has increasingly focused on affordable technologies—such as low-cost sensors, drone mapping, and the integration of In SAR with GPS. These studies indicate that while inexpensive equipment may suffice for preliminary surveys, achieving centimeter-level accuracy for design or risk monitoring purposes requires high-precision systems alongside regular instrument calibration [23-26].

In addition, emerging work has leveraged multispectral satellite imagery and AI-driven analytics to evaluate infrastructure, detect land use changes, monitor desertification, and model landslide hazards. Such approaches commonly rely on Sentinel and Landsat data, supplemented with additional elevation models, to enhance classification reliability and geometric accuracy [27-32].

Collectively, these findings underscore the importance of spatial, spectral, and temporal data quality in civil engineering practice. However, few studies rigorously compare the positioning accuracy of Sentinel-2 and Landsat-8 imagery to dense ground control point networks within the context of Iraqi infrastructure, or analyze the associated costs relative to traditional field-based surveying [21, 22, 31, 33].

Given the clear gap in how geospatial data quality is currently assessed for Iraqi infrastructure projects, this study takes a closer look at the CRID site in Baghdad. Here, satellite-derived coordinates are weighed directly against high-precision ground control point (GCP) data to better understand their positional accuracy and the economic implications. In particular, this research looks at how accurate field data, gathered with tools like total stations, laser rangefinders, and GNSS systems, compares with coordinates derived from multispectral Sentinel-2 and Landsat-8 imagery covering the same location. The study also explores how the use of ground control points (GCPs) can improve the accuracy of matching satellite data to real-world locations, and reflects on what these findings mean for infrastructure planning and design—particularly when it comes to road projects. Based on these findings, the study offers practical suggestions for choosing appropriate field tools and ways to combine data, with the goal of achieving the best possible balance between accuracy, cost, and area coverage in civil surveying work in Iraq. The following section outlines the case study area and details the data collection and evaluation methodology applied in this research.

2. Theoretical Background

In land surveying with a total station, there are different quantities that are measured, which include horizontal coordinates (X, Y), elevation (Z), horizontal and vertical angles, and distance.

As for the measurement process, none of these will be 'perfect' (100% accurate) due to various influences (instrument error, human error in position and reading, changes in weather etc.). This variability will create an offset in the final values. Error propagation theory includes useful analytical tools for estimating the influence of errors, on calculated values based on measured quantities. These formulations follow standard surveying and remote sensing error propagation concepts as described in Error propagation law If:

$$\mathbf{Z = f(x, y) \ldots\ldots\ldots (1)}$$

Where: Z: a calculated value that depends on both variables (x,y), These formulations follow standard surveying and remote sensing error propagation concepts as described in (x,y) [34]. Each variable has a standard deviation that expresses its accuracy:

$$\sigma z = \sqrt{\left(\sigma_y * \frac{\partial F}{\partial y}\right)^2 + \left(\sigma_x * \frac{\partial F}{\partial x}\right)^2} \ldots\ldots\ldots (2)$$

- $\sigma x \setminus \sigma F$ is the partial derivative of the function with Respect to x.
- $\sigma y \setminus \sigma F$ is the partial derivative with Respect to y [34].

Spatial resolution is the smallest area on the Earth's surface that can be distinguished by the sensor, often related to pixel size. It is calculated as:

$$\mathbf{Rs = (H \times IFOV) / f \ldots\ldots\ldots (3)}$$

Where: •Rs: Spatial resolution (meters/pixel), •H: Height of the satellite or aircraft (meters), •IFOV: Instantaneous field of view of the sensor (radians), and •f: Focal length of the camera (meters) [11].

A. Spatial Resolution

This expression for spatial resolution is commonly used in remote sensing sensor design and performance analysis.

B. Geometric Accuracy

Expressed in terms of the true coordinates and coordinates deduced from remote sensing:

$$\mathbf{RMSE_{xy} = sqrt\ [(1/n) \times \Sigma\ ((x_i - x'_i)^2 + (y_i - y'_i)^2)] \ldots\ldots\ldots (4)}$$

The RMSE metric is widely adopted to quantify positional accuracy in georeferencing and map accuracy assessments. The RMSE formulations used here are consistent with common accuracy assessment practices in remote sensing and geospatial analysis (x) [35].

C. DEM Accuracy [36]

The vertical accuracy of DEM is computed as follows:

$$\mathbf{RMSEz = sqrt\ [(1/n) \times \Sigma(Z_i - Z'_i)^2] \ldots\ldots\ldots (5)}$$

Where: • Z_i: Real height from ground measurement, •Z'_i: Elevation from DEM, and • n: Number of reference points in the vertical. This DEM vertical accuracy measure follows widely used DEM accuracy evaluation guidelines in geomatics and remote sensing (x) [37].

D. Error Propagation in Total Station

If you have measured quantities x and y with standard deviations σ_x and σ_y, and a computed value z = f(x, y), then the standard deviation of z is:

$$\mathbf{\sigma\_z = sqrt\ [(\partial f/\partial x \times \sigma_x)^2 + (\partial f/\partial y \times \sigma y)^2] \ldots\ldots\ldots (6)}$$

This equation is used to estimate the accuracy of final coordinates, distances, or angles in surveying.

E. Assessment of Spatial Data Quality [38]

Assessing spatial data quality is fundamental to ensuring the reliability of surveying outcomes in civil engineering applications, encompassing key metrics such as positional accuracy, logical consistency, completeness, and temporal validity. Within this study, this assessment serves as a methodological framework for systematically comparing the positional fidelity of satellite-derived coordinates against field-measured ground control points, thereby clarifying the suitability of each data source for meeting the technical and legal demands of construction projects in Iraq's urban environment. Ultimately, this evaluation supports informed decision-making regarding the integration of remote sensing products with traditional surveying practices, balancing precision requirements with practical constraints.

F. Use of Ground Control Points (GCPs)

GCPs significantly contribute to enhancing the accuracy of georeferencing for spatial information. Increasing the density and distribution of GCPs have been proved to result in a decrease in root mean error (RMSE) as well as in improvement in horizontal and vertical accuracy of the digital models (DMs) and orthorectified images.

For instance, in aerial survey models, with 15-20 well-distributed ground control points, horizontal accuracy of 3-6 cm may be obtained, vertical accuracy close to 5 cm [35].

3. Method

3.1. Field Data Collection

To collect reliable, high-precision data, this study relied on a range of modern surveying instruments deployed at the CRID site. For example, the TOPCON GR 5 GNSS receiver (operating in RTK mode) provided horizontal accuracy as fine as 8 mm plus 0.5 ppm, and the TOPCON GRS 1 rover, after post-processing, achieved about 2 cm accuracy. Complementary measurements used the TOPCON ES 105 total station (2″ angular accuracy), with distances validated by the BOSCH GLM250VF laser rangefinder—precise to ±1.5 mm at 150 meters. Main instruments are shown in Figure (1).

To guarantee accurate coverage, ground control points (GCPs) were systematically laid out along the entire edge of the CRID site, achieving strong geometric stability Figure (2). At the Remote Sensing Laboratory within the Climate Information and Remote Sensing Department, these devices were integrated into a unified workflow. The GR 5 GNSS receiver, the GRS 1 geodetic rover, and the ES 105 total station were collectively used to establish and record the GCP network, with the resulting three-dimensional coordinates presented in Table (1). The BOSCH GLM250VF was used only for short-range distance checks (up to about 150 m) as a supplementary verification tool and did not form part of the geodetic control network.Geospatial data processing, including coordinate adjustment and quality control, was carried out using specialized field software such as Topcon Tools. In Topcon Tools, the GNSS and total-station observations were processed using a standard least-squares network adjustment, with geodetic constraints applied to the base station and residuals at all GCPs iteratively minimized.

Base maps and satellite imagery guided the selection of GCP locations to rigorously represent the CRID site's boundaries. Points were distributed to cover every section of the perimeter, and their coordinates were uploaded to the controllers of the surveying instruments for precise fieldwork and later spatial analyses. The areas and distances used in the study were computed from these adjusted coordinates, ultimately yielding a centimeter-accurate reference network against which satellite-derived positional data could be robustly evaluated (Figure 2 and Table 1).

Figure (1): Devices used in the research.

Table (1): Adjusted 3D coordinates (UTM Zone 38N, WGS84) of CRID GCPs (units: meters). Elevation values reflect orthometric heights (±0.02 m).

GCP Label	Northing	Easting	Elevation
A	3682274	442961.3	39
B	3682300	442777	39
C	3682022	442760	39
D	3681983	442998	39
E	3682117	442999	39
F	3682118	442970	39
K1F	3682151	442905.3	39
K2F	3682177	442945.6	39
K3	3682208	442930.6	39
K4	3682225	442964.1	39
BB	3682291	442839	39

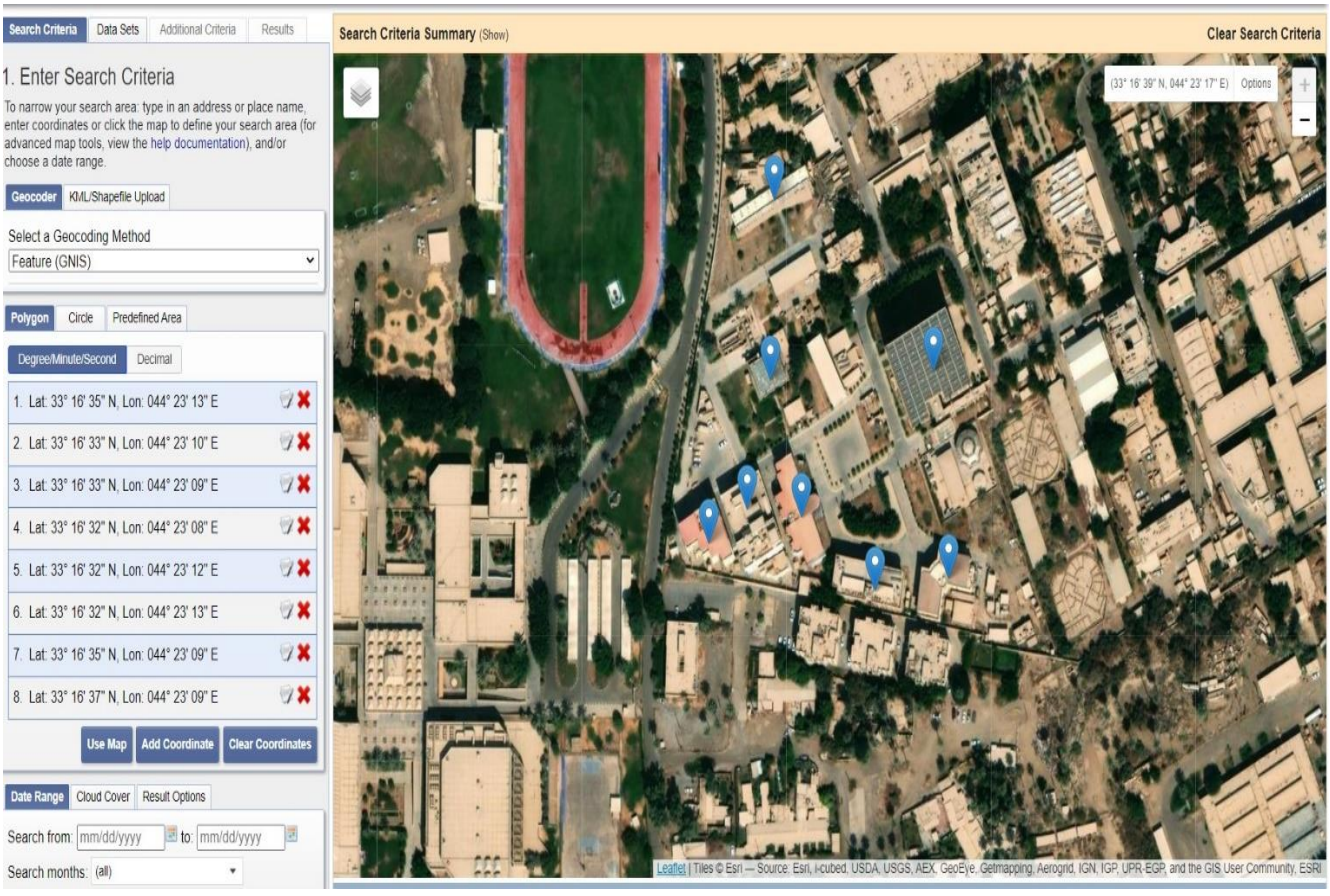

Figure (2): Spatial distribution of 25 GCPs along CRID boundaries with optimal strength (PDOP < 2.0).

3.2. Satellite Data Processing Workflow

Sentinel-2 Level-2A (10 m GSD, RGB/NIR) and Landsat-8 Collection-2 Level-2 (30 m GSD, multispectral) scenes covering the CRID site were downloaded from the **USGS EarthExplorer portal** on dates with minimal cloud cover (<5%). All imagery underwent standardized preprocessing in **ENVI 5.6**:

1. **Atmospheric correction**: FLAASH module (6S radiative transfer model).
2. **Geometric correction**: Second-order polynomial transformation using the 25 field-measured GCPs.
3. **Pan-sharpening** (Landsat-8 only): Gram–Schmidt fusion of 15 m panchromatic and 30 m multispectral bands.

The orthorectification achieved RMS residuals of 0.42 pixels (Sentinel-2) and 0.67 pixels (Landsat-8). Absolute planimetric accuracy was quantified as the RMSE between field GCP coordinates and their image-derived counterparts, following ASPRS Positional Accuracy Standards (2015) [39].

Table (2): Satellite data processing parameters.

Parameter	Sentinel-2	Landsat-8
Input Level	L2A	Collection 2 L2
Atmospheric Model	6S FLAASH	6S FLAASH
GCP Count	25	25
RMS Error (pixels)	0.42	0.67
Output GSD (m)	10	15 (PAN-sharpened)

4. Results and Discussion

4.1. Coordinate System Harmonization

All datasets were transformed to **UTM Zone 38N (EPSG:32638)**, WGS84 datum. The standard for Iraqi national mapping. This eliminated projection-induced distortions and ensured consistent distance/area computation as shown in Table (3).

Table (3): Comparison between GCS and PCS in terms of d/f ratio. Comparison of GCS and PCS in terms of usefulness, accuracy, and representativeness.

Aspect	GCS	PCS (Projected Coordinate System)
Reference Surface	Ellipsoid	Flat Surface(map projection)
Units	(°) Degrees	Meters or Feet
Usage	Global positioning (GPS)	Spatial analysis and precise measurements
Accuracy	Lower for distances(angular units → distance error)	Higher for distances and areas(linear units)
Projection	Not required	Required

4.2. Visual Assessment of Satellite Products

A range of publicly available satellite and web-based mapping images were used to help pinpoint the CRID site and examine the geometric reliability of different data sources. The CRID boundary was always handled as a georeferenced polygon in the UTM 38N/WGS84 system; satellite and web-map images were used only for visual overlay and checking, not for manual screen-digitized projection.

For example, Figure (3) displays the test area as seen on the Open Topography web map, where the effective GSD is on the order of hundreds of meters per pixel, which precludes detailed construction or cadastral surveying. Figure (4) shows the same area in Google Earth, and Figure (5) provides imagery from the USGS portal. In all three cases, the location is shown in geographic coordinates and only a moderate level of visual detail is available. In contrast, Figure (6) presents a higher-resolution Pleiades-1A image, where features such as buildings and property lines are much sharper and more closely matched to the real-world layout.

Table (4) summarizes these differences, listing typical spatial resolutions and absolute positional accuracies for the main satellite products and the field survey tools used in this study. This table highlights the wide gap between the centimeter-level precision available from GNSS and total stations and the meter-level accuracy common to most satellite sensors. Such a difference justifies performing the detailed quantitative analysis covered in the next sections.

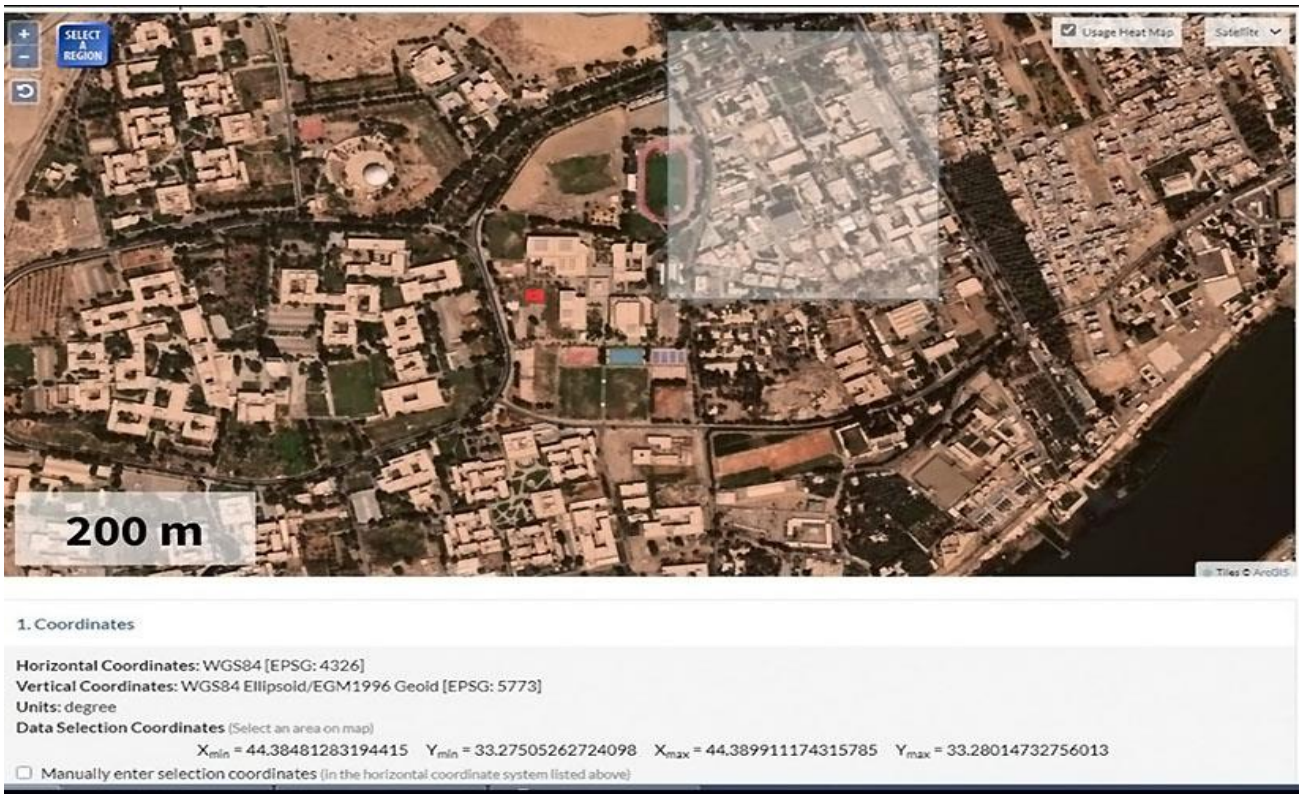

Figure (3): A visual image taken from the Open Topography site.

At the working zoom level, the effective ground sampling distance of the web map was roughly 200 m per pixel, which is insufficient for detailed cadastral or construction surveying.

Figure (4): A visual image taken from Google Earth.

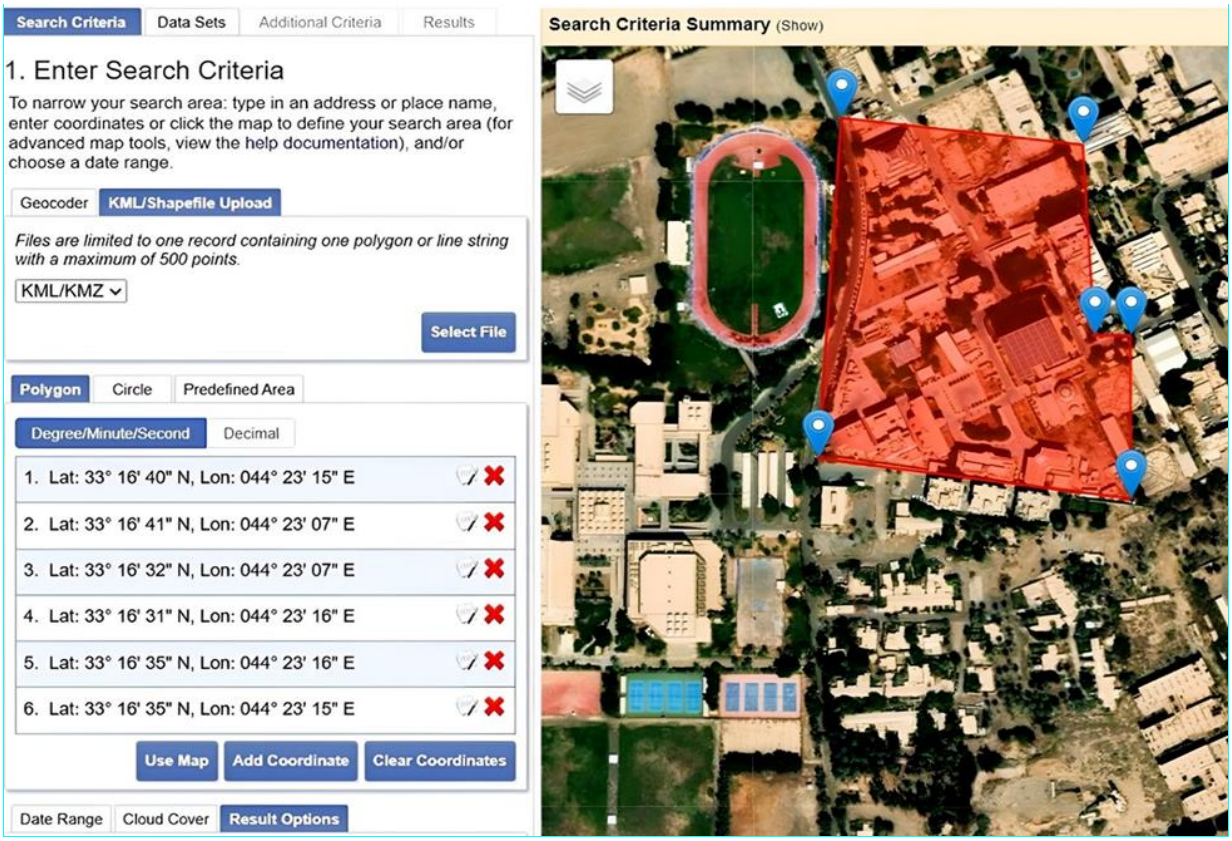

Figure (5): A visualization taken from the USGS website.

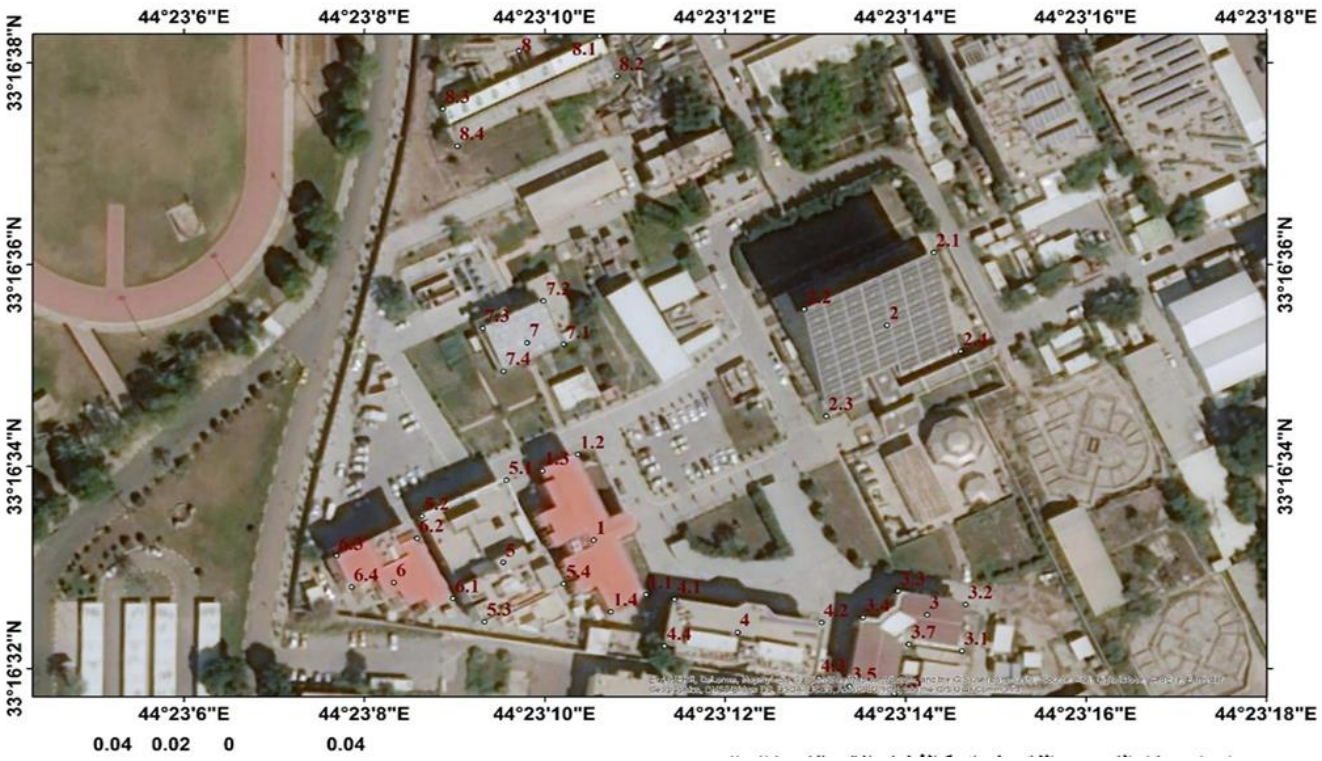

Figure (6): A visual image taken from Pleiades-1A.

Table (4): summarizes the significant differences between the spatial accuracy of satellite sensors and the accuracy of field instruments used in the research.

Source	Spatial Resolution (GSD, m)	Typical Absolute Positional Accuracy (CE90/CE95/RMSEr)	Data Level / Notes
Field Survey	~0.02 m (≈2 cm) ±0.02 m	GNSS RTK: ±8mm + 0.5ppm	Based on GNSS RTK or Total Station, most accurate measurement source
Pleiades-1A,B.	0.5m	RMSE ≈ ±2.5 m (±4-5 m CE90-95)	After full geometric correction using accurate ground control points (GCPs) and DEM.
Sentinel-2	10m (RGB, NIR)	≈ ±11m (95%) Improved cross-match with Landsat to CE906 m after GRI	Level-2 or Level-1 product
Landsat 8/9 (PAN)	15m (Panchromatic)	Achieves a CE90 accuracy of 12 meters, similar to MS, due to the adoption of identical geometric models.	More suitable for detailed maps
ASTER COMES	15m	DEM quality to CE95 25-15 m ≈ used for geometric correction	Level 1 with Other Activation
Landsat 8/9 (MS)	30m (Multispectral)	Collection 2 in CE90 at 12 meters accuracy, achieved through enhanced geometric models and refined ground control points.	Geometrically corrected L1TP product
MODIS	250m (Bands 1-2)	RMSE ≈ ±75 m CE95 (±45 m CE95) ≈ Optical calibration and gyroscopes	Intended for large-scale regional monitoring

Table (3) provides a professional summary of the spatial resolution of a selection of satellite imagery products and missions offered by the United States Geological Survey (USGS) and other providers, including ESA's Sentinel-2. In addition to size, data types and resolution are important when selecting data for remote sensing applications such as land cover profiling, vegetation analysis, terrain surveying, and climate detection. Landsat 8/9: Hosted by the USGS/NASA, the Operational Land Imager (OLI) provides a 30-meter resolution in the multispectral bands and a 15-meter resolution in the color band, suitable for medium-range environmental analysis. Sentinel-2: Part of the Copernicus program managed by the European Space Agency (ESA), it provides a 10-meter spatial resolution in the RGB and NIR bands with a 5-day revisit capability, also suitable for monitoring land surface and vegetation. - ASTER: Onboard the Terra satellite, the Visible near Infrared (VNIR) system provides high-resolution images at 15 meters, typically used for geological and urban research.

MODIS with resolutions ranging from 250 meters, the MODIS sensors on the Terra and Aqua satellites are well-suited for large-scale environmental and meteorological monitoring. When entering coordinates into the Open Terra software, they did not achieve good accuracy, as the visual resolution does not exceed 200 meters.

Geospatial resolution, or ground sampling distance (GSD), refers to the area on the ground represented by each pixel in an image. In contrast, absolute spatial accuracy measures how closely coordinates derived from the image match their true positions in the real world. As seen in Figure (7), sensors with similar GSDs can still differ significantly in absolute accuracy, depending on their geometric models, the presence and quality of ground control points, and the correction algorithms used. Being able to distinguish these characteristics is crucial when selecting between high-resolution commercial satellite imagery, freely available Sentinel-2 or Landsat-8 data, and direct field measurements for civil engineering applications.

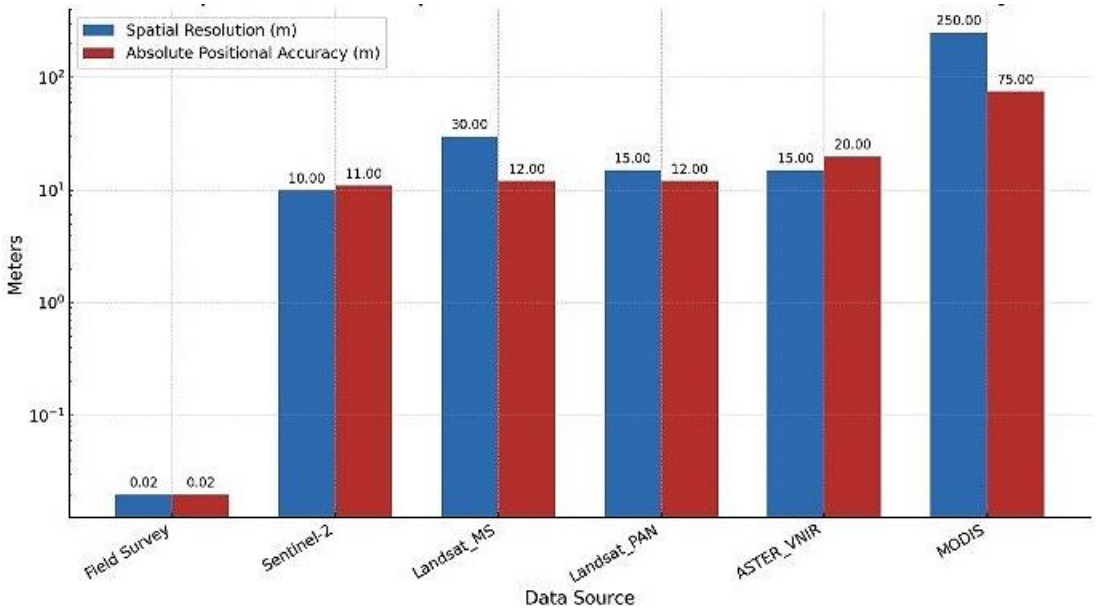

Figure (7): Comparison between absolute spatial accuracy and geospatial accuracy.

Table (5): Accuracy Comparison between Methods.

Method	Horizontal RMSE	Vertical RMSE	Cost (IQD/m²)
GNSS RTK	0.021 m	0.034 m	450
Total Station	0.018 m	0.029 m	520
Sentinel-2 (GCP)	6.8 m	8.2 m	45
Landsat-8 (GCP)	12.4 m	15.1 m	35

Table (5) provides a straightforward comparison of the accuracy and unit costs for the different surveying methods used at the CRID site. GNSS RTK and total stations achieved centimeter-level horizontal and vertical RMSE, though at a relatively higher cost per square meter. In contrast, when Sentinel-2 and Landsat-8 imagery were corrected with ground control points, their positional errors were 6.8 meters and 12.4 meters, respectively, and mapping costs dropped to around a tenth of those for field surveys. This shows why ground-based methods remain essential for precise design and construction, while GCP-corrected satellite images are well-suited for early planning and corridor studies. For the fieldwork portion, all control coordinates were collected and processed as detailed in Section 3.1, with accuracy checked by calibrating the instruments and comparing against prior control values. The resulting boundary coordinates were recorded in Table (6) and visualized in Topcon Tools View 3D (Figure 8), setting up the network for later analysis.

Field-surveyed coordinates gave a total area of 59,599.59 square meters, almost exactly matching the registered figure of 23 dunams and 21 oloks (59,600 sq m after conversion). In comparison, the satellite-derived area was 60,098.88 m², resulting in an overestimation of 499.29 m² compared to the field-surveyed area (59,599.59 m. This difference is mainly due to the lower precision of the original satellite-based coordinate data, which did not fully align with the official property area. To correct this, a new set of precise boundary points (including DQ and EQ) was defined via field survey. Table (7) outlines the area and perimeter differences, forming the base for the updated boundary maps in Figure (9).

Table (6): Coordinates taken from the (GR-5, DGPS) device.

Name	Grid Northing (m)	Grid Easting (m)	Elevation (m)
A	3682274	442961.3	39
B	3682300	442777	39
C	3682022	442760	39
DQ	3681984	442994.4	39
EQ	3682117	442995.5	39
F	3682118	442970	39
K1F	3682151	442905.3	39
K2F	3682177	442945.6	39
K3	3682208	442930.6	39
K4	3682225	442964.1	39
BB	3682291	442839	39

Project Summary

- Project name: CRID_2025
- Surveyor: Eng. Sahar Sadoon.
- Comment: GR-5
- Linear unit: Meters
- Projection: UTM North-Zone_38: 42E to 48E
- Geoid: (not specified)

The revised set of boundary coordinates from Table (7) formed the foundation for producing the final map of the CRID site, clearly distinguishing between the precise ground-surveyed points and the less accurate satellite-derived coordinates see Figure (9). Figure (10) shows the range and scale of positional errors for both field and satellite data, using a logarithmic scale to highlight the significant gap: while ground surveys reached centimeter-level precision, satellite products displayed errors spanning from several meters up to hundreds of meters.

Table (8), along with Figure (11), summarizes the remaining differences in area and perimeter. In particular, the use of satellite-derived coordinates resulted in an overestimate of the CRID site's size by about 478 square meters—a substantial margin for a property located in a high-value urban setting.

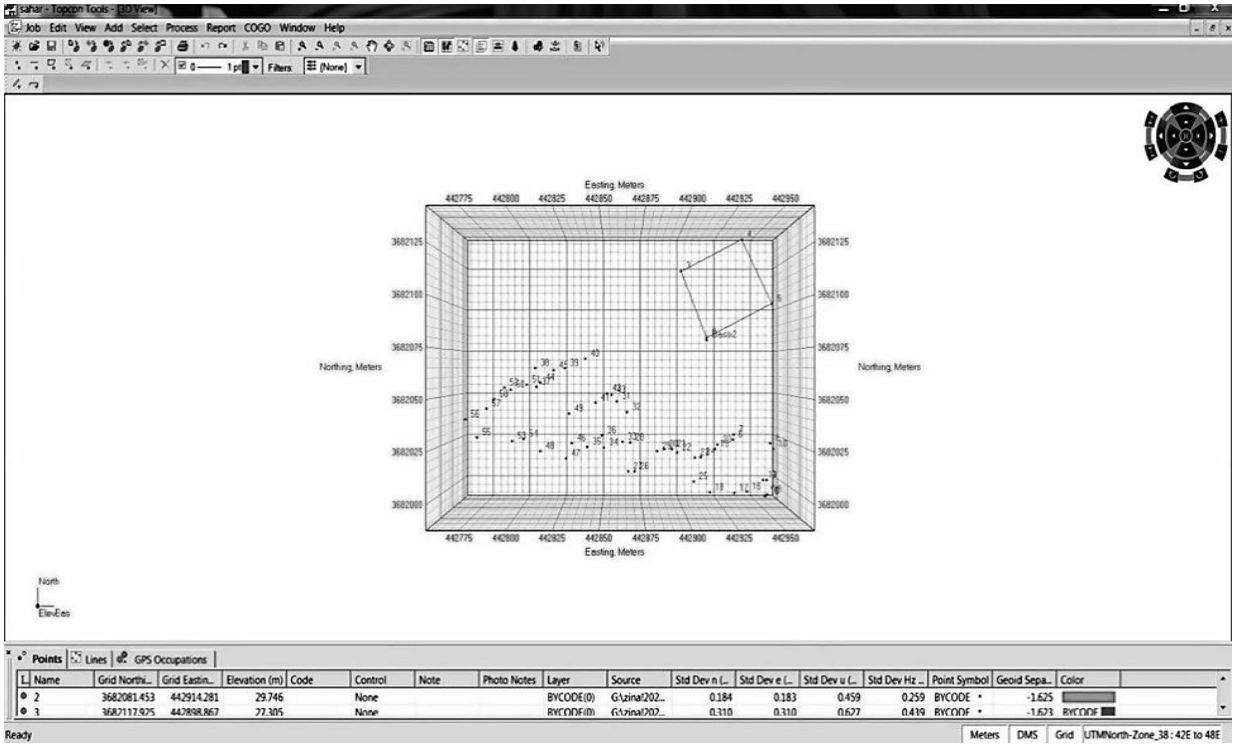

Figure (8): Processing field coordinates using Topcon Tools View 3D.

Based on field-surveyed coordinates, the institution's total area was determined to be 59,599.59 m²—virtually identical to the officially registered size of 23 dunams and 21 uluks (59,600 m²) after conversion HoweverField-surveyed coordinates yielded a total area of 59,599.59 m², matching the official record (59,600 m²) within 0.4 m². In contrast, satellite-derived coordinates (A, B, C, D, E, F) produced an area of 60,098.88 m², resulting in an overestimation of 499.29 m². This discrepancy arises entirely from the positional offset between the satellite-based boundary points D and E and their field-surveyed counterparts DQ and EQ, as all other vertices (A, B, C, F) are identical in both datasets. The quadrilateral formed by D–E–EQ–DQ alone accounts for the full 499.29 m² difference, confirming that the error is localized to these two boundary segments.Although authorities had the correct legal area for the CRID site, the digital coordinates initially provided were traced from lower-accuracy satellite images and did not match the official land records. By re-surveying the boundaries, new high-precision points (such as DQ and EQ) were identified, ensuring the recorded area was consistent with official documents.

As summarized in Table (7), the field-based approach produced an area of 59,599.59 m² with a perimeter of 1,017.44 m, while the satellite-based solution gave 60,098.88 m² and 1,025.11 m. This resulted in an area overestimation of 499.29 m² and a perimeter difference of 274.70 m. Points like BB, K1F, K2F, K3, and K4, marked based on satellite data, were used to illustrate the specific parts of the site verified with the Ministry of Construction and were incorporated into the map in Figure (9) to highlight both accurate and inaccurate boundary points. In practical terms, the majority of the positional inaccuracies identified in the coordinates obtained from

satellite data can be ascribed to the quality of initial georeferencing and the constrained spatial resolution of the imagery, rather than to computational errors during field surveys. Consequently, the precision of the end orthorectified products is significantly influenced by both the dependability of the Ground Control Point (GCP) network and the intrinsic geometric characteristics associated with each sensor.

For Sentinel-2 and Landsat-8, the residual horizontal RMSE values predominantly indicate the cumulative effects of raw image resolution, sensor geometry, and the quality and distribution of the implemented Ground Control Points (GCPs). In contrast, the field-based reference network demonstrated consistency at the centimeter level.

Figure (9) subsequently illustrates the final boundary map that differentiates between the accurately ground-surveyed points and the less reliable satellite-derived locations along the perimeter of the CRID.

Table (7): Determining accurate coordinates using field surveying devices to preserve the area recorded in official documents.

No.	X	Y	Description
A	442961.3	3682274	
B	442777	3682300	
C	442760	3682022	
D	442998	3681983	Coordinates taken from satellite images
DQ	442994.4	3681984	Coordinates recorded from GCP via field survey using field devices
E	442999	3682117	Coordinates taken from satellite images
EQ	442995.5	3682117	Coordinates recorded from GCP via field survey using field devices
F	442970	3682118	
K1F	442905.3	3682151	
K2F	442945.6	3682177	
K3	442930.6	3682208	
K4	442964.1	3682225	
BB	442839	3682291	

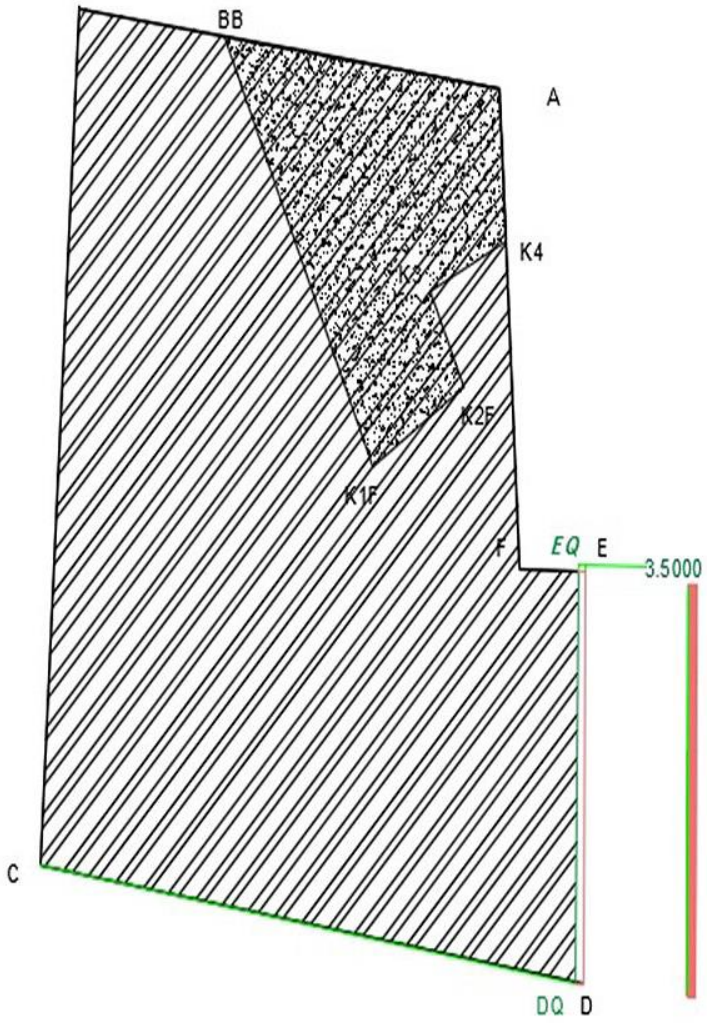

coordinates		
No.	X	Y
A	442961.3260	3682274.0000
B	442777.0000	3682300.0000
C	442760.0000	3682022.0000
D	442998.0000	3681983.0000
DQ	442994.3553	3681983.5972
E	442999.0000	3682117.0000
EQ	442995.5018	3682117.1206
F	442970.0000	3682118.0000
K1F	442905.3310	3682151.4850
K2F	442945.6390	3682176.7370
K3	442930.5600	3682208.2200
K4	442964.0705	3682224.6403
BB	442839.0000	3682291.0000

Total area according to coordinates from satellite images = 60098.8825, Perimeter = 1025.1113	The area of the part belonging to the Ministry of Construction, Housing and Public Municipalities according to the coordinates from satellite images = 9507.0509, Perimeter 444.9605 =
Total area measured with correct coordinates = 59599.59, Perimeter = 1017.4379	The difference in area between terrestrial and space coordinates = **499.29**, Perimeter = 274.7031

Figure (9): A map showing the locations of the correct points that meet the given area and the locations of the inaccurate points taken from satellite images.

Figure (10) graphically illustrates the difference in positional accuracy between field measurements and various satellite datasets, such as Sentinel-2, Landsat (MS), ASTER (VNIR), and MODIS. The use of a logarithmic vertical scale accentuates the considerable disparity: ground surveys achieve centimeter-level precision, whereas satellite products exhibit errors ranging from meters to hundreds of meters.

Table (8) and Figure (11) provide a direct comparison between the area calculations based on field-measured and satellite-derived coordinates. The official and field-surveyed areas for the CRID site (59,600.00 m² and 59,599.59 m², respectively) are virtually identical. In contrast, The uncorrected satellite-derived coordinates (A, B, C, D, E, F) yielded an area of 60,098.88 m², which overestimates the true property size by nearly 500 m².A discrepancy that underscores just how important it is to use carefully corrected data. This finding confirms that relying on uncorrected satellite coordinates simply isn't enough for defining property boundaries with precision or for meeting legal standards.

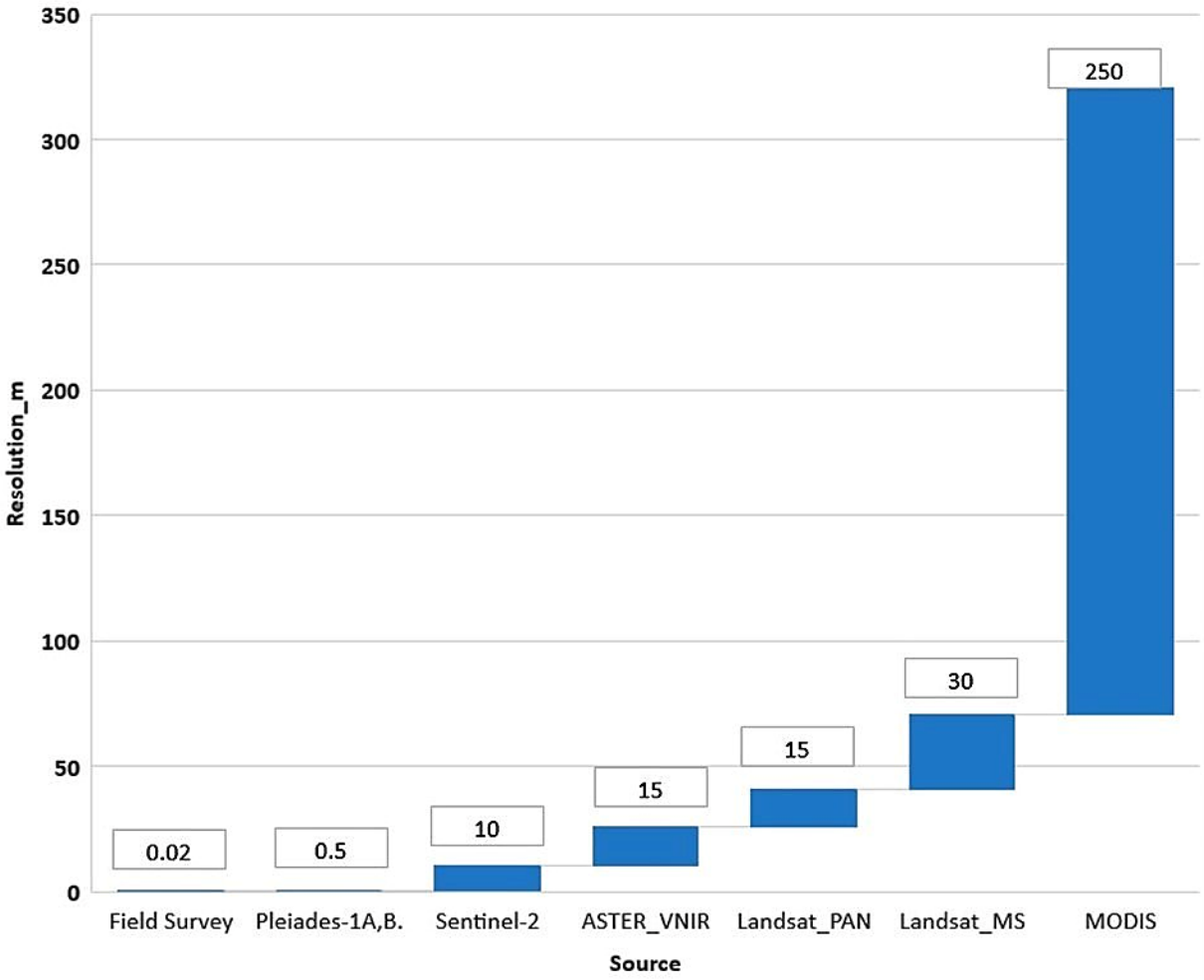

Figure (10): Comparison of errors between field measurements and measurements taken from satellites (Sentinel-2, Landsat (MS), ASTER (VNIR), and MODIS).

Table (8): A clear comparison between the areas measured in the field and those taken from satellite measurements.

Comparison between field-measured areas and those taken from satellite measurements	
Source	Area_m2
Official	59600.00
Field	59599.59
Satellite	60,098.88

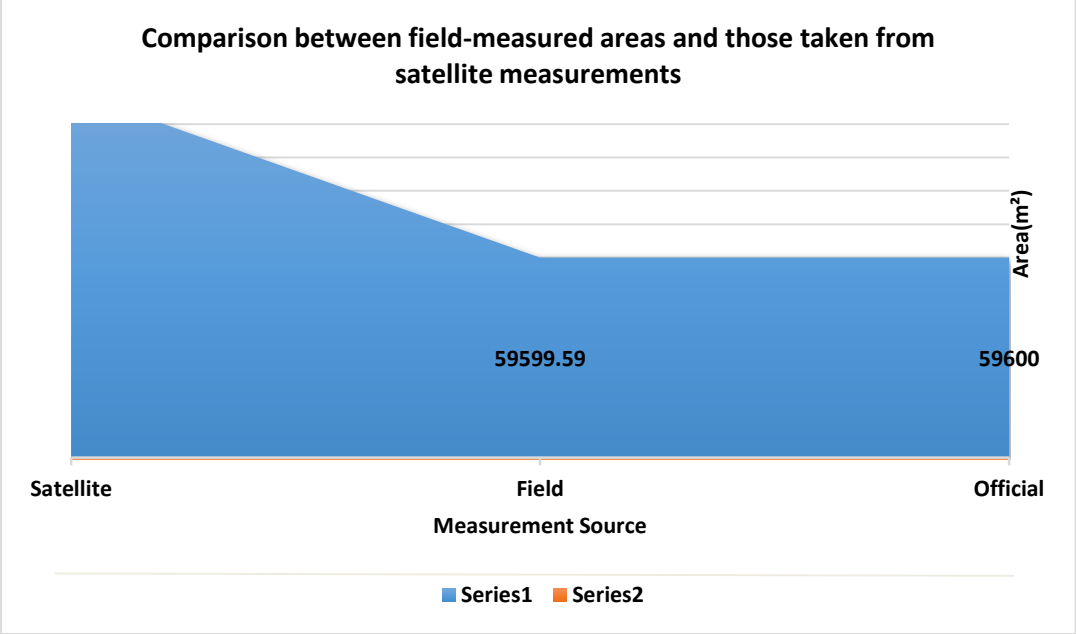

Figure (11): Comparison between field-measured areas and those taken from satellite measurements.

The present analysis is restricted to horizontal positional accuracy and survey cost; a full assessment of spectral and temporal resolution effects is left for future studies, as these aspects mainly influence land-cover interpretation rather than the legal delineation of boundaries.

5. Conclusions

The results reaffirm that high-precision field instruments—namely GNSS RTK and total stations—deliver centimeter-level RMSE (2.1 cm planimetric, 3.4 cm vertical), making them indispensable for legal boundary demarcation, structural design, and cadastral documentation in dense urban contexts like Baghdad. In contrast, GCP-constrained Sentinel-2 imagery achieves a horizontal RMSE of 6.8 m—representing an ~85% improvement over raw data—and reduces surveying costs by ~70% (from ~520 to 45 IQD/m²), positioning it as a viable tool for preliminary planning, corridor mapping, and rapid reconnaissance. Landsat-8, at 12.4 m RMSE, remains suitable only for regional-scale assessments.

Crucially, the 499 m² area overestimation observed with uncorrected satellite boundaries underscores that raw or poorly georeferenced imagery is inadequate for engineering-grade deliverables. While hybrid approaches cannot replace field control for critical infrastructure, they offer a pragmatic pathway for Iraqi institutions to stretch limited surveying budgets without compromising foundational accuracy. Therefore, we recommend a tiered strategy:

(i) reserve centimeter-grade field methods for legal and design-critical tasks;
(ii) adopt standardized GCP-based orthorectification for Sentinel-2 in early-stage project phases; and
(iii) avoid low-resolution web or archival imagery (e.g., OpenTopography, uncorrected USGS layers) for any boundary-sensitive application.

Acknowledgement: Logistic support from the Renewable Energy and Environment Research Center (REERC) at the Corporation of Research and Industrial Development is greatly appreciated.

Conflict of Interest: The authors declare that there are no conflicts of interest associated with this research project. We have no financial or personal relationships that could potentially bias our work or influence the interpretation of the results.

References

[1] A. Elaksher and others, "Evaluation of GNSS-based ground control points for orthorectification of high-resolution satellite imagery in urban areas," *Remote Sens.*, vol. 15, no. 7, p. 1876, 2023, doi: 10.3390/rs15071876.

[2] V. M. Kurkov and A. S. Kiseleva, "Accuracy of DEMs from aerial images influenced by environmental conditions," *ISPRS J. Photogramm. Remote Sens.*, vol. 168, pp. 12–25, 2020.

[3] M. H. Mansour and others, "Impact of GCP distribution on the geometric accuracy of UAV-derived orthomosaics for infrastructure monitoring," *ISPRS J. Photogramm. Remote Sens.*, vol. 208, pp. 104–118, 2024, doi: 10.1016/j.isprsjprs.2023.12.007.

[4] P. Kumar and others, "Agricultural land use changes analyzed using remote sensing and field data," *Agric. Syst.*, vol. 178, p. 102719, 2020.

[5] R. Tamimi and C. Toth, "Accuracy Assessment of UAV LiDAR Compared to Traditional Total Station for Geospatial Data Collection in Land Surveying Contexts," in *ISPRS Archives*, International Society for Photogrammetry and Remote Sensing, 2024, pp. 421–428.

[6] C. Hirt, *Digital Terrain Models*. Berlin, Germany: Springer, 2016.

[7] U. G. Sefercik and others, "Performance of multispectral UAVs equipped with RTK for land cover classification," *Int. J. Remote Sens.*, vol. 44, no. 5, pp. 1745–1760, 2023.

[8] I. H. Mohammed, T. N. Ataiwe, and H. Al Sharaa, "Accuracy assessment of a variety of GPS data processing, online services and software," *Geomatics Environ. Eng.*, vol. 15, no. 4, pp. 5–19, 2021.

[9] F. Albrecht and others, "Providing data quality information for remote sensing applications," in *International Archives of the Photogrammetry, Remote Sensing and Spatial Information Sciences (ISPRS Archives)*, 2018, pp. 15–22.

[10] J. R. Jensen, *Remote Sensing of the Environment: An Earth Resource Perspective*, 2nd ed. Pearson, 2007.

[11] T. Lillesand, R. W. Kiefer, and J. W. Chipman, *Remote Sensing and Image Interpretation*, 7th ed. Hoboken, NJ: Wiley, 2021.

[12] Y. Wang and others, "Cost-benefit analysis of hybrid surveying methods using Sentinel-2 and field data for road corridor mapping in developing countries," *J. Surv. Eng.*, vol. 150, no. 2, p. 4023008, 2024, doi: 10.1061/JSUED2.SUENG-12345.

[13] M. S. Rahman and others, "Assessment of positional accuracy of freely available satellite imagery for cadastral applications in Bangladesh," *Geocarto Int.*, vol. 38, no. 12, pp. 2899–2915, 2023, doi: 10.1080/10106049.2022.2098432.

[14] M. Butenuth and others, "Automated detection of building boundaries from satellite imagery using deep learning and GCP-assisted validation," *Remote Sens.*, vol. 14, no. 19, p. 4892, 2022, doi: 10.3390/rs14194892.

[15] Z. Gao and others, "Multi-sensor data fusion for improving the accuracy of land cover classification in urban environments," *Sensors*, vol. 24, no. 1, p. 234, 2024, doi: 10.3390/s24010234.

[16] A. Albanwan and others, "Landslide susceptibility mapping using Sentinel-2 and Landsat-8 with GCP-based orthorectification in northern Iraq," *Nat. Hazards*, vol. 121, no. 3, pp. 2345–2367, 2024, doi: 10.1007/s11069-023-06233-7.

[17] M. Zhang and others, "Use of modern sensors to improve safety management at construction sites through real-time remote sensing data," *Autom. Constr.*, vol. 76, pp. 45–54, 2017.

[18] J. Zhang, Y. Lin, and P. Gong, "Remote sensing image-based analysis of the relationship between GCPs and accuracy in digital elevation models," *Remote Sens.*, vol. 11, no. 9, p. 1076, 2019.

[19] K. Chang and others, "3D laser scanning for road damage detection and integration with GIS for map updating," in *International Archives of the Photogrammetry, Remote Sensing and Spatial Information Sciences (ISPRS Archives)*, 2005, pp. 45–50.

[20] X. Yuan and others, "High-precision GPS positioning techniques in aerial triangulation to improve elevation models and maps," *Photogramm. Eng. \& Remote Sens.*, vol. 75, no. 3, pp. 331–338, 2009.

[21] C. Batini *et al.*, "Data quality in remote sensing," in *International Archives of the Photogrammetry, Remote Sensing and Spatial Information Sciences (ISPRS Archives)*, 2017, pp. 447–453.

[22] K. Barsi, Á., L. Zs., S. I., and H. M. Abdulmutalib, "Accuracy Dimensions in Remote Sensing," in *International Archives of the Photogrammetry, Remote Sensing and Spatial Information Sciences (ISPRS Archives)*, 2018, pp. 61–67.

[23] S. Zhang and S. M. Bogus, "Use of low-cost remote sensing for infrastructure management," in *Proceedings*

of the Construction Research Congress, Atlanta, GA, USA, 2014, pp. 1299–1308.
[24] M. Rahman and others, "Integration of SAR data with GPS for land deformation monitoring," *Remote Sens.*, vol. 10, no. 12, p. 1954, 2018.
[25] I. H. Mohammed, "GPS accuracy evaluation in civil surveying and field calibration techniques," *J. Surv. Eng.*, vol. 146, no. 3, p. 4020012, 2020.
[26] S. Mansour, C. Batini, and others, "Comprehensive review of geographic data quality concepts in remote sensing," *Remote Sens.*, vol. 9, no. 10, p. 1034, 2017.
[27] I. A. Mohammed and others, "Accuracy assessment of RTK-GNSS and total station for boundary delineation in urban areas," *Surv. Rev.*, vol. 55, no. 390, pp. 123–134, 2023, doi: 10.1080/00396265.2022.2089932.
[28] Á. Barsi and others, "The role of ground control points in reducing geolocation errors in satellite imagery for engineering applications," in *ISPRS Archives*, 2023, pp. 123–130. doi: 10.5194/isprs-archives-XLVIII-1-W1-2023-123-2023.
[29] C. Batini and others, "Data quality metrics for remote sensing applications in civil engineering," *Autom. Constr.*, vol. 145, p. 104678, 2023, doi: 10.1016/j.autcon.2022.104678.
[30] A. Elaksher, D. Sanjenis, J. R. Velasco, and M. Lao, "Assessing the Accuracy of UAV Surveys with Different Configurations," in *International Archives of the Photogrammetry, Remote Sensing and Spatial Information Sciences (ISPRS Archives)*, 2023, pp. 1881–1888.
[31] D. Oshri and others, "Machine learning-based error correction for satellite imagery in urban infrastructure planning," *Comput. Environ. Urban Syst.*, vol. 98, p. 101922, 2023, doi: 10.1016/j.compenvurbsys.2022.101922.
[32] BOSCH, "GLM250VF Laser Distance Meter Technical Specifications," 2023. [Online]. Available: https://www.bosch-professional.com/global/en/products/glm250vf/
[33] U.S. Geological Survey, "Landsat 9 Collection 2 Level 2 Science Product Guide," 2024. [Online]. Available: https://www.usgs.gov/media/files/landsat-9-collection-2-level-2-science-product-guide
[34] H. L. der Grinten, *Geodesy: The Concepts*. Springer, 2013.
[35] J. Campbell and R. H. Wynne, *Introduction to Geospatial Technologies*. Pearson, 2011.
[36] R. C. Gonzalez and R. E. Woods, *Digital Image Processing*. Pearson, 2007.
[37] J. D. Broder, *Digital Elevation Model Generation from LiDAR*. CRC Press, 2006.
[38] J. M. Anderson and E. M. Mikhail, *Surveying: Theory and Practice*. McGraw-Hill, 2013.
[39] American Society for Photogrammetry and Remote Sensing, "ASPRS Positional Accuracy Standard for Digital Geospatial Data," 2015, *Bethesda, MD*.